phys. stat. sol. (a) **201**, No. 7, 1563–1569 (2004) / **DOI** 10.1002/pssa.200306807

Magnetic properties and magnetic domain structure of bulk glass forming $Nd_{60}Al_{10}Fe_{20}Co_{10}$ alloy

B. C. Wei[*, 1], **G. S. Yu**[1], **W. H. Li**[2], **W. Löser**[3], **S. Roth**[3], and **J. Eckert**[3, 4]

[1] Institute of Mechanics, Chinese Academy of Sciences, Beijing 100080, P.R. China
[2] Institute of Materials, Shanghai University, Shanghai 200072, P.R. China
[3] IFW Dresden, Institut für Metallische Werkstoffe, Postfach 270016, 01171 Dresden, Germany
[4] Present address: FB Material und Geowissenschaften, FG Physikalische Metallkunde, Technische Universität Darmstadt, Petersenstr. 23, 64297 Darmstadt, Germany

Received by Martin S. Brandt 12 August 2003, revised 6 March 2004, accepted 12 March 2004
Published online 11 May 2004

PACS 61.43.Dq, 75.50.Kj, 75.70.Kw, 81.05.Kf

The transition from hard to soft magnetic behaviour with increasing quenching rate is shown for $Nd_{60}Al_{10}Fe_{20}Co_{10}$ melt-spun ribbons with different thickness. Microstructure and magnetic domain structure of ribbons were studied by magnetic force microscopy (MFM). Particle sizes <5 nm decreasing gradually with increasing quenching rate were deduced from topographic images which differ from large-scale magnetic domains with a periodicity of about 350 nm in all ribbons irrespective the coercivity. This indicates that the magnetic properties of the alloy are governed by interaction of small magnetic particles. It is concluded that the presence of short-range-ordered structures with a local ordering similar to the A1 metastable Nd–Fe binary phase is responsible for the hard magnetic properties in samples subjected to relatively low quenching rate.

1 Introduction

Recently, bulk metallic glasses (BMGs) obtained in multicomponent (Nd,Pr)–Fe based systems have attracted great attention due to their high coercivity and the absence of glass transition before crystallization in isochronal differential scanning calorimetry (DSC) measurements [1–9]. The reason for the high coercivity was presumed to be the presence of a relaxed disordered structure that can be regarded as an ensemble of Nd(Pr)–Fe and Nd(Pr)–Fe–Al clusters with large random magnetic anisotropy [2, 4–6]. However, so far hard magnetic behaviour was not detected in melt-spun ribbons of composition identical with BMG and moreover, it seems that high coercivity can not be achieved by annealing [2, 4, 8, 9]. The effect of heavier rare earth (RE) elements Sm, Dy and Gd substitution for Nd and Pr on the magnetic properties of the $Nd(Pr)_{60}Fe_{30}Al_{10}$ BMG was also studied [10, 11]. However, the RE-rich Sm(Dy,Fe)–Fe based metallic glasses, where Sm(Dy,Gd)–Fe clusters may exist, did not show hard magnetic properties at room temperature, irrespective of the quenching rate applied. Furthermore, the Nd-rich Nd–Al–Co system displayed paramagnetic properties at room temperature, though the presence of Nd–Co clusters is also possible [2, 12]. Consequently, the mechanisms responsible for the hard magnetic properties of the Nd(Pr)-based BMGs and the relationship between microstructure and magnetic properties are still not clear.

In this work, the effect of quenching rate on magnetic behaviour of $Nd_{60}Al_{10}Fe_{20}Co_{10}$ alloys is studied. Ribbons with thickness ranging from 30 to 200 μm have been prepared by melt spinning at different wheel speeds, which bridge the gap between hard magnetic as-cast BMG samples and rapidly quenched

[*] Corresponding author: e-mail: weibc@imech.ac.cn, Tel.: 86-10-62614945, Fax: 86-10-62615524

ribbons displaying low coercivity. The magnetic properties are related to microstructure and magnetic domain structure, and the magnetic hardening mechanism is discussed.

2 Experimental

Ingots of $Nd_{60}Al_{10}Fe_{20}Co_{10}$ were prepared by arc-melting a mixture of the pure elements Nd, Al, Fe and Co with a purity of at least 99.9% in a titanium-gettered argon atmosphere. Ribbons were obtained by melt-spinning using a single copper wheel under pure argon atmosphere. The surface speed of the copper wheel was varied from 3 to 18 m/s, and the corresponding thickness of the ribbon varies from 200 to 32 μm. The structure of the melt-spun ribbons was characterized by X-ray diffraction (XRD) using CoK_α radiation. Thermal analysis was performed with a Perkin–Elmer DSC 7 differential scanning calorimeter under argon atmosphere. A heating rate of 0.33 K/s was employed to reveal the crystallization and melting behaviour. The magnetic polarization as a function of the magnetic field was measured at room temperature using an alternating-gradient magnetometer (AGM) with maximum applied field of 1592 kAm^{-1}. The Curie temperatures were measured with a Faraday magnetometer at a heating rate of 0.17 K/s. The study of the domain structure was carried out by using a Digital Instruments NanoScope IIIa D-3000 magnetic force microscope (MFM). It allows the topographic and magnetic force images to be collected separately and simultaneously in the same area of the sample by using Tapping/Lift modes. The magnetic tips used were micro-fabricated Si cantilevers with a pyramidal tip coated with magnetic Co–Cr thin film of 40 nm thickness and a coercivity of about 32 kAm^{-1}. In our experiments, the tip used was magnetized downward prior to imaging. Its lift-height during scanning was 30 nm. Further details regarding the MFM experiments are given in Ref. [13]. The ribbons were studied on their non-contact side without any pre-treatment.

3 Results and discussion

DSC results for the samples are shown in Fig. 1. The sharp exothermic peak with an onset temperature (T_x) around 750 K in all traces corresponds to the massive crystallization of the amorphous phase. This is in accordance with the XRD results, which show that all the ribbons melt-spun at different speeds comprise a large fraction of amorphous phase. A small exothermic peak starting from about 472 K is observed in ribbons prepared at surface speeds of 12 m/s and higher. This is suggested to be an early step of crystallization, as isothermal annealing at 453 K gives rise to a bell-shape exothermal peak, indicating that both nucleation and growth processes proceed [14].

As can be seen in Fig. 2, the profile of hysteresis loops of $Nd_{60}Al_{10}Fe_{20}Co_{10}$ amorphous ribbons changes with increasing wheel speed. The coercivity (H_c) decreases gradually from 180 kA/m to 30.5 kA/m with the wheel speed increasing from 3 m/s to 18 m/s. The saturation magnetization under external field of 1592 kAm^{-1} (J_{1592}), and remanent magnetization (J_r) slope down continuously with rising quenching rate, from 0.156 T and 0.087 T for the 3 m/s ribbon to 0.100 T and 0.020 T for the 18 m/s ribbon, respectively. A typical thermomagnetic plot is shown in Fig. 3. The dependence of the

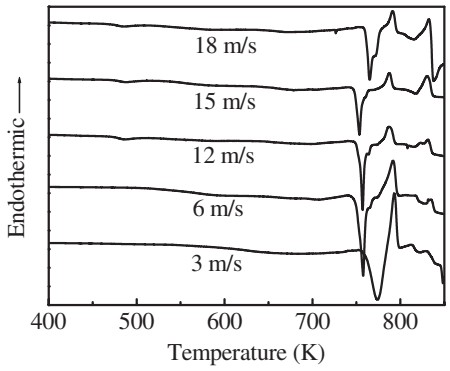

Fig. 1 DSC curves of $Nd_{60}Al_{10}Fe_{20}Co_{10}$ ribbons melt-spun at different speed.

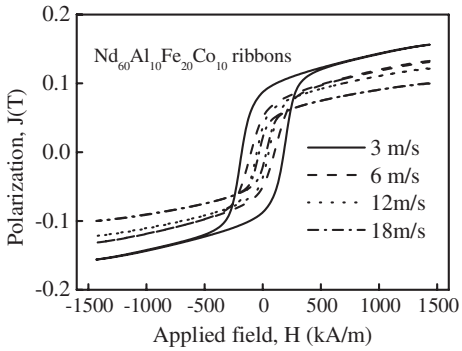

Fig. 2 *J*–*H* hysteresis loops for $Nd_{60}Al_{10}Fe_{20}Co_{10}$ ribbons melt-spun at different speed.

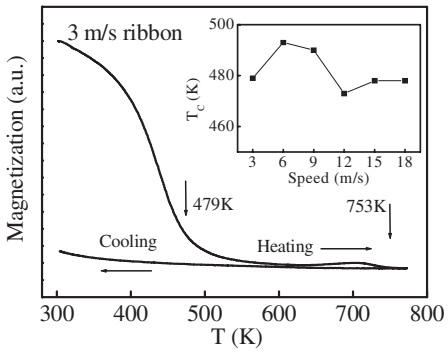

Fig. 3 Thermomagnetic analysis of the ribbon melt-spun at 3 m/s; Inset: Curie temperature T_c vs. wheel rotating speed.

Curie temperatures on the wheel speed is shown in the inset to Fig. 3. The sample thickness and the magnetic properties of the melt-spun ribbons at room temperature are listed in Table 1, along with T_x and the onset temperature of melting (solidus temperature, T_m) determined by DSC measurements. The magnetic properties and the tendency of coercivity to decrease with increasing quenching rate are in accordance with other results on Nd–Fe metallic glass systems [2, 4, 8, 9, 12].

A study of the magnetic domain structure is useful for understanding the micromagnetic mechanisms. Here, a MFM was employed to image the magnetic domain structure in ribbons with different quenching rates and, consequently, different coercivities. In Fig. 4a topographic (left) and magnetic force (right) images of the ribbon melt-spun at 3 m/s are presented. Nanoscale particles embedded in the matrix are observed in the topographic image. The corresponding magnetic force image is characterized by darker areas adjacent with brighter areas of sub-micron scale and a random distribution. The dark area indicates that the magnetization direction in this area is nearly parallel to the upward tip magnetization, and the bright area indicates the opposite. This kind of magnetic contrast is similar to our previous results on Nd-based BMG but the magnetic force contrast in the ribbon is lower than that in a cast bulk sample [13]. The average periodicity (L) of the domain pattern and the average contrast between dark and bright areas were measured by means of section analysis, revealing $L \approx 360$ nm, the maximum phase shift $\Delta\phi_{max}$ (represents the magnetic force) is 3.54 degrees, and the root mean square (RMS) of the magnetic force is 0.226 degrees. In a higher magnification image (Fig. 4b) of the ribbon melt-spun at 3 m/s, the average lateral size 40 nm of the particles was determined by using section analysis. The lateral width of the isolated particles in the topographic image is, in fact, enlarged by the tip when the size of the particle is smaller than the radius of the tip (the tip radius is about 20 nm in present study), while the vertical height can measure the true size of a particle [15]. It is found that the average size of the particles is about 5 nm by averaging the heights of the particles. This size agrees well with our recent high resolution transmission electron microscopy results, where a large number of isolated nanocrystals with an average diameter

Table 1 Magnetic and thermal properties of $Nd_{60}Al_{10}Fe_{20}Co_{10}$ ribbons melt spun at different speed.

melt-spinning speed (m/s)	thickness (μm)	H_c (kA/m)	J_{1592} (T)	J_r (T)	T_c (K)	T_m (K)	T_x (K)
3	199	180	0.156	0.087	479	~776	759
6	121	100	0.130	0.050	493	778	750
12	50	50.7	0.121	0.037	473	779	752
15	39	40.1	0.112	0.027	478	780	748
18	32	30.5	0.100	0.020	478	786	760

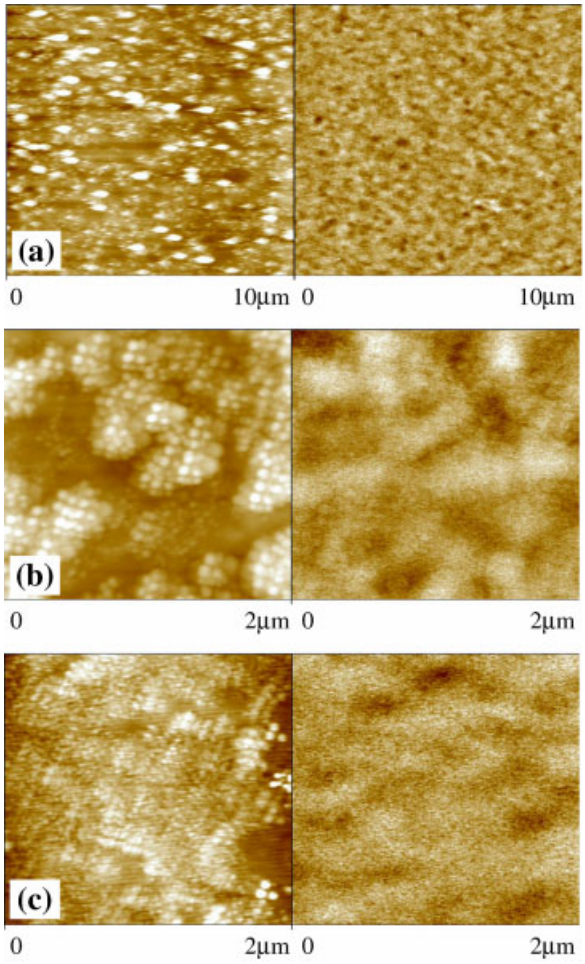

Fig. 4 (online colour at: www.interscience.wiley.com) Topographic (left) and MFM (right) images of as-spun $Nd_{60}Al_{10}Fe_{20}Co_{10}$ ribbon melt-spun at 3 m/s (a), 3 m/s (high resolution images) (b), and 12 m/s (c).

about 5 nm was observed [16]. This means that the particle size in the topographic MFM images reflects the microstructure of the ribbon surface. The corresponding magnetic force image (Fig. 4b) clearly shows that the size of the magnetic domains is much larger than the size of the particles. This indicates that the large areas of magnetic contrast are actually a collection of a group of particles with similar magnetic orientation. The isolated particles are correlated by some kind of interaction with each other.

With the increase of the wheel speed, the size of the particles in the topographic images decreases gradually. Figure 4c presents the topographic and magnetic force images of the ribbon melt-spun at 12 m/s. The average size of particles in the topography image is about 1.4 nm determined by section analysis. This is much smaller than the particles found for the ribbon melt-spun at 3 m/s. In the magnetic force image (Fig. 4c), dark and bright domains are also observed. Section analysis of magnetic force images in low magnification shows that L = 350 nm, $\Delta\phi_{max}$ = 2.19 degrees, and *RMS* = 0.215 degrees for the 12 m/s sample. When the melt-spinning speed attains 18m/s, no particles can be distinguished in the matrix of the ribbon. However, the presence of long range magnetic order in the ribbon with a domain periodicity of about 350 nm is also observed in the magnetic force image. $\Delta\phi_{max}$ and *RMS* decrease to 1.98 degrees and 0.20 degrees, respectively.

In order to reveal the ferromagnetic mechanism of the present Nd–Fe–Al–Co metallic glass, one has to consider the magnetic properties of crystalline or partially crystalline Nd-rich Nd–Fe binary alloys. It has been known since long that as-cast Nd-rich alloys in the Fe–Nd system show high coercivity (H_{ci} = 320–400 kA/m). Croat has proposed that a high coercivity in Nd–Fe alloys rapidly quenched at a relatively low cooling rate is probably due to the formation of one or more metastable crystalline Nd–Fe phases [17]. Owing to the important role of the binary Nd–Fe eutectic in governing the magnetic properties of Nd–Fe–B permanent magnets, the mechanism responsible for the hard properties and microstructure of Nd-rich Nd–Fe binary alloys have later been studied in detail. Most of these results support that the high coercivity can be attributed to the presence of a metastable highly anisotropic A1 phase [18–24]. This phase was not identified in XRD spectra, but its presence has been confirmed by thermomagnetic analysis (TMA). The Curie temperature of the A1 phase is near 513 K [17–24]. Though a lot of work including high resolution transmission electron microscopy (HRTEM) [23, 24], TEM [22], neutron diffraction and Mössbauer spectrometry [21] has been done, the composition and the crystal structure of this phase have not been determined exactly, yet. The composition of the A1 phase was reported to be

Nd_3Fe_7 [18], $NdFe_{1.1}$ [19], $NdFe_4O$ [20] or between $NdFe_4$ and Nd_2Fe_3 [23, 24] by different authors, while the structure was reported to be cubic, tetragonal, or amorphous [18–24]. The identification of the A1 phase is difficult as it is formed as a nano-scale eutectic structure [22–24]. The addition of aluminium to the Nd–Fe binary eutectic greatly enhances the glass forming ability (GFA), and the addition of cobalt into the Nd–Fe–Al system further improves the GFA [1, 5]. Therefore, the widely distributed crystalline Nd particles in thick ribbons of Nd–Fe alloys [17–24], were not observed in the present melt-spun metallic glass. Moreover, it is well known that amorphous materials lack long-range order but otherwise have appreciable chemical short-range order (CSRO) that often resembles that of a related equilibrium or metastable crystalline phase. Hence, the magnetic properties of most amorphous alloys should be comparable to those of the corresponding crystalline phase (or phases). It is not easy to give a definite border line between nanocrystals and clusters with SRO. We term both of them as SRO structure here. We can not give a direct structural evidence for the existence of the A1 phase in the present alloy yet. However, our MFM results confirm the presence of a large number of nano-scale particles in the ribbons. These particles may comprise nano-scale A1 phase and Nd. TEM and HRTEM results also prove the presence of some unknown nano-scale phases in the ribbons and BMG of similar systems [2, 13, 25]. The magnetic properties of the present thick ribbons and bulk samples [13] are indeed similar to Nd–Fe binary alloys [17–24]. Consequently, we suggest that the presence of a SRO structure, which has a similar local structure as the A1 phase in Nd–Fe binary alloys, is responsible for the hard magnetic properties in samples subjected to relatively low quenching rates (ribbons melt-spun at 3 or 6 m/s in the present work). Some indirect evidence supports this opinion. Delamare et al. [22] have studied the possibility of the formation of the Al phase in RE–Fe (RE = La to Lu) systems by calculating the formation enthalpy, in which the solidification mechanism of a Nd–Fe eutectic alloy leads firstly to a Nd + $NdFe_2$ metastable equilibrium, and secondly to A1 (with Nd contents within 20 ~ 40%) + Nd equilibrium phase by phase dissociation of $NdFe_2$ [22]. It was concluded that all RE-Fe systems other than Nd–Fe and Pr-Fe exhibit positive values of the formation enthalpy, and the absence of the A1 phase. The only presence of the A1 phase in the Nd–Fe and Pr-Fe systems is in accordance with the results for RE-based BMGs, i.e. a high coercivity at room temperature is only found for the Nd–Fe and Pr-Fe based systems. Other systems, such as Sm(Dy,Gd)-Fe-based alloys and Nd-Co alloys without iron show soft magnetic and paramagnetic properties, respectively [2, 10–12]. Further evidence is given by the magnetic study of ball-milled powder in a similar alloy system, where the alloy ball-milled for 60 hours shows the typical features for an amorphous phase in XRD, but exhibits paramagnetic properties at room temperature [12]. The ball-milled powder is considered as a disordered packing of different atoms without special CSRO (purely glassy material). The significant difference of magnetic properties between the as-quenched alloys and ball-milled powders indicates that the local structure of the amorphous phase for the different experimental conditions is significantly different. This suggests that the ferromagnetic properties in the present metallic glass are due to the presence of SRO structures similar to the A1 phase in the Nd–Fe binary system.

Another question concerns the mechanism for the coercivity which decreases continuously with the increase of quenching rate as shown in Fig. 2. The spin coupling and the magnetic anisotropy are expected to be strongly dependent on the composition. The difference in coercivity measured at room temperature may, therefore, be related to different compositions obtained as the quenching rate varies [9]. A highly relaxed Fe-enriched SRO can form in the thick ribbons due to the relative low quenching rate. However, this is not the only reason in the present alloy. The Curie temperature (T_c) of the ribbons melt-spun at different speeds, which is sensitive to local chemical composition, does not show a distinct tendency of decreasing with increasing quenching rate (inset in Fig. 3), though the strong tendency of coercivity to decrease with increasing quenching rate is indeed observed (Fig. 2 and Table 1). For example, the 3 m/s ribbon and the 18 m/s ribbon exhibit almost the same T_c, but the coercivities are 180 and 30.5 kA/m, respectively. A Mössbauer spectroscopy study of a similar alloy showed that the samples prepared at different quenching rate all comprise a non-magnetic amorphous phase, and much more Fe atoms were found to be non-magnetic in rapidly quenched samples [25]. Low coercivity and magnetization values in the thinner ribbons are also associated with the presence of a larger fraction of nonmagnetic amorphous phase. The present alloys are hard to be magnetized to saturation (Fig. 2) due to the

noncollinear sperimagnetic structure, which is likely to exist in glassy rare earth-Fe alloys [26, 27]. Croat et al. [17] supposed that in Nd–Fe binary alloys, a paramagnetic effect is responsible for the decrease of coercivity at higher quenching rate, where magnetically isolated A1 phase particles are dispersed in a paramagnetic crystalline Nd matrix. This non-interaction model is not sufficient to interpret the magnetic behaviour of the present alloy. It should be noted that the magnetic structure study of the present alloy displays a typical interaction-type domain structures as shown in Fig. 4 [28]. This indicates that there are interactions between SRO clusters. The anisotropic short-range-ordered structures are aligned by the ferromagnetic coupling between nanosize clusters. The behaviour of the magnetization curves in similar alloy system reported by others also give some hint on the presence of clusters and strong interactions between them [11, 26, 29]. Based on the sizes of the SRO structures revealed by MFM and the coercivities (Tab. 1) for ribbons melt-spun at different speed, the obtained coercivity dependence on the diameter (D) of the SRO structures follows a rough dependence of $H_c \propto D^1$. In materials consisting of magnetic particles in a conducting (nonmagnetic) medium, the possibility exists of a reduced exchange coupling between the grains [30]. However, the effects of these interactions are in general complex and not easy to prove. Furthermore, the magnetic characteristics of the amorphous matrix in the alloy are still not clear. From the thermomagnetic curves of the ribbons (Fig. 3), one can see that above T_c the magnetization does not decrease to zero until about 753 K. This phenomenon can also be observed in results of Inoue et al. [2], indicating that a second magnetic phase may exist in the alloy. Hence, competing magnetic interactions may account for the complex magnetic properties of the alloy. This category probably comprises spin glasses, antiferromagnets, superparamagnets and some ferromagnets. The mechanism for the interactions needs further study.

4 Conclusion

In conclusion, the magnetic properties of $Nd_{60}Al_{10}Fe_{20}Co_{10}$ ribbons are sensitive to the quenching rate. High coercivity is revealed for the thick ribbons (exceeding 100 μm), with a value lower than that in bulk samples of the same composition, whereas thin ribbons are magnetically soft [13]. The MFM images show particles with a size of about 5 nm in the ribbon melt-spun at 3 m/s. Therefore, short-range-ordered structures possessing a local chemical order similar to the metastable A1 phase known from the Nd–Fe binary system, which are supposed to be responsible for the hard magnetic properties in thick ribbons. The size of the short-range-ordered structures decreases strongly with the increase of spinning speed. Large-scale magnetic domains with a periodicity of about 350 nm are observed in all ribbons melt-spun irrespective the wheel speed. The anisotropic short-range-ordered structures are aligned by the magnetic interactions.

Acknowledgements The authors are grateful to A. Yan, Z. G. Sun and G. Kumar for stimulating discussions. This work was supported by the National Nature Science Foundation of China (Grant Nos. 50101012), and the Deutsche Forschungsgemeinschaft (DFG) through Sonderforschungsbereich 463 and Schwerpunktprogramm 1120.

References

[1] A. Inoue, T. Zhang, A. Takeuchi, and W. Zhang, Mater. Trans. JIM **37**, 636 (1996).
[2] A. Inoue, A. Takeuchi, and T. Zhang, Metall. Mater. Trans. A **29**, 1779 (1998).
[3] Y. Li, S. C. Ng, Z. P. Lu, Y. P. Feng, and K. Lu, Phil. Mag. Lett. **78**, 213 (1998).
[4] J. Ding, Y. Li, and W. Z. Wang, J. Phys. D: Appl. Phys. **32**, 713 (1999).
[5] L. Q. Xing, J. Eckert, W. Löser, S. Roth, and L. Schultz, J. Appl. Phys. **88**, 3565 (2000).
[6] G. J. Fan, W. Löser, S. Roth, J. Eckert, and L. Schultz, Appl. Phys. Lett. **75**, 2984 (1999).
[7] B. C. Wei, Y. Zhang, Y. X. Zhuang, D. Q. Zhao, M. X. Pan, W. H. Wang, and W. R. Hu, J. Appl. Phys. **89**, 3529 (2001).
[8] H. Chiriac and N. Lupu, J. Non-Cryst. Solids **287**, 135 (2001).
[9] R. J. Ortega-Hertogs, A. Inoue, and K. V. Rao, Scr. Mater. **44**, 1333 (2001).
[10] G. J. Fan, W. Löser, S. Roth, and J. Eckert, Acta Mater. **48**, 3823 (2000).
[11] H. Z. Kong, J. Ding, Z. L. Dong, L. Wang, T. White, and Y. Li, J. Phys. D: Appl. Phys. **35**, 423 (2002).

[12] G. Kumar, J. Eckert, L. Q. Xing, A. Güth, S. Roth, W. Löser, and S. Ram, Mat. Res. Soc. Symp. Proc. Vol. **644** L12, 14 (2001).
[13] B. C. Wei, W. H. Wang, M. X. Pan, B. S. Han, Z. R. Zhang, and W. R. Hu, Phys. Rev. B **64**, 012406 (2001).
[14] L. C. Chen and F. Spaepen, Nature **24**, 336 (1988).
[15] Y. J. Chen, W. Y. Cheung, I. H. Wilson, N. Ke, S. P. Wong, J. B. Xu, H. Sang, and G. Ni, Appl. Phys. Lett. **72**, 2472 (1998).
[16] L. Xia, B. C. Wei, M. X. Pan, D. Q. Zhao, W. H. Wang, and Y. D. Dong, J. Phys.: Condens. Matter **15**, 3531 (2003).
[17] J. J. Croat, J. Appl. Phys. **52**, 2509 (1981).
[18] J. Strzeszewski, A. Tsoukatos, and G. C. Hadjipanayis, J. Appl. Phys. **67**, 4966 (1990).
[19] K. G. Knoch, B. Grieb, E. Th. Henig, H. K. Kronmüller, and G. Petzow, IEEE Trans. Magn. **26**, 1951 (1990).
[20] J. L. S. Llamazares, F. Leccabue, F. Bolzoni, R. Panizzieri, and X. R. Hua, J. Magn. Magn. Mater. **84**, 79 (1990)
[21] D. Givord, J. P. Nozières, M. F. Rossignoal, D. W. Taylor, I. R. Harris, D. Fruchart, and S. Miraglia, J. Alloys Compd. **176**, L5 (1991).
[22] J. Delamare, D. Lemarchand, and P. Vigier, J. Alloy Comp. **216**, 273 (1994).
[23] V. P. Menushenkov, A. S. Lileev, M. A. Oreshkin, and S. A. Zhuravlev, J. Magn. Magn. Mater. **203**, 149 (1999).
[24] V. P. Menushenkov, S. J. Andersen, and R. Høier, Proceedings of the 10th International Symposium on Magnetic Anisotropy and Coercivity in Rare-Earth Transition Metal Alloys, Dresden, Werkstoff-Informationsgesellschaft, 97 (1998).
[25] L. Wang, J. Ding, Y. Li, Y. P. Feng, X. Z. Wang, N. X. Phuc, and N. H. Dan, J. Magn. Magn. Mater. **224**, 143 (2001).
[26] R. S. Turtelli, D. Triyono, R. Grössinger, H. Michor, J. H. Espina, J. P. Sinnecker, H. Sassik, J. Eckert, G. Kumar, Z. G. Sun, and G. J. Fan, Phys. Rev. B **66**, 054441 (2002).
[27] R. C. Taylor, T. R. McGuire, J. D. Coey, and A. Gangulee, J. Appl. Phys. **49**, 2885 (1978).
[28] M. A. Al-Khafaji, W. M. Rainforth, M. R. J. Gibbs, H. A. Davies, and J. E. L. Bishop, J. Magn. Magn. Mater. **182**, 111 (1998).
[29] G. Kumar, J. Eckert, S. Roth, K.-H. Müller, and L. Schultz, J. Alloys Compd. **348**, 309 (2003).
[30] R. W. Chantrell, N. Walmsley, J. Gore, and Maylin, Phys. Rev. B **63**, 024410 (2000).